ACS APPLIED ENERGY MATERIALS

Open Access

www.acsaem.org

Article

p-Type Thermoelectricity of CrN Thin Films by Mg Doping

Published as part of ACS Applied Energy Materials special issue "Solid-State Structural Design for Energy Conversion and Storage".

Takashi Aizawa,* Frank F. Yun, and Takao Mori*

Cite This: *ACS Appl. Energy Mater.* 2025, 8, 13360−13366

Read Online

ACCESS | Metrics & More | Article Recommendations | Supporting Information

ABSTRACT: Because of the high power factor of chromium nitride (CrN) when used in thin films, it has recently attracted widespread attention as a promising high-performance thermoelectric material. Several reports have described studies of alloying or doping of CrN thin films to control and enhance the thermoelectric properties. Most reported CrN thin films have been fabricated as n-type charge carriers. Recent reports have described that nitrogen deficiency and alloying with V or W enhance n-type behavior and increase the power factor. Although V has fewer valence electrons than Cr, it has been shown not to change the carrier polarity. Our measurements have revealed that Mg-doped CrN thin films deposited using the reactive magnetron sputtering method change the polarity to p-type charge carriers, which is consistent with our calculations. The maximum observed power factors of the fabricated ∼8% Mg-alloyed CrN thin-film samples were 0.6 mW·m^{-1}·K^{-2} at room temperature to 0.9 mW·m^{-1}·K^{-2} at approximately 550 K.

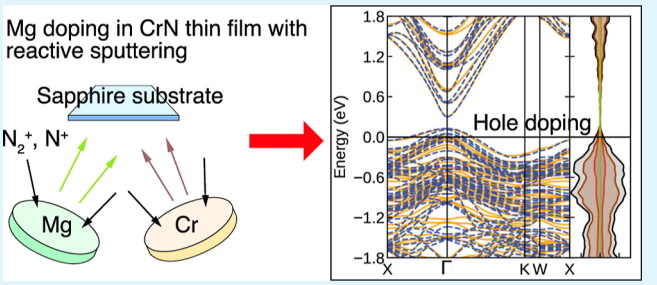

KEYWORDS: *Crn, sputtering, thin film, epitaxy, Mg, doping, p-type, DFT*

1. INTRODUCTION

The development of ubiquitous, small, electronic Internet of things (IoT) devices has created tremendous demand for highly efficient portable power sources to drive them.[1] Thin-film thermoelectric (TE) power generators are promising candidates to satisfy such demand for power sources.[2−5] Transition-metal nitride thin films have attracted widespread attention[6] recently because of hosting several desirable characteristics for these applications. Among them, chromium nitride (CrN) is particularly promising because it provides the following benefits. First, the films have a large Seebeck coefficient with high electrical conductivity corresponding to a large power factor (PF), which suggests a high power generation potential. Second, the in-air stability of CrN thin films obviates additional protective procedures needed for application purposes. Third, compared to conventional thermoelectric materials such as Bi_2Te_3, the abundance and reduced toxicity of CrN elemental components make them cost-efficient and safe. Finally, CrN thin films can be fabricated easily using reactive sputtering.[7−18] Such methods are well-known as fast and efficient fabrication processes. Combined, these benefits of efficient power generation, safe, and cost-effective elemental raw materials and rapid fabrication make this material highly desirable for many applications.

After formation, CrN is a rock-salt (B1) type crystal with a near-zero indirect band gap (E_g) of 0.19 ± 0.46 eV.[11] As measured optically, the direct E_g value is 0.64−0.7 eV.[7,11] These properties of electronic structure indicate that CrN is suitable for use as a TE material at approximately room temperature (RT) or higher. Several CrN thin-film fabrication methods have been reported: reactive sputtering,[7−18] plasma-assisted molecular beam epitaxy (PA-MBE),[19,20] and pulsed-laser deposition (PLD).[21] As a substrate, using MgO(100), which has the same rock-salt crystal structure and well-matched lattice constant at a = 421.4 pm, allows CrN to grow epitaxially in a cube-on-cube manner.[7,8,11,12,16,19−21] Actually, that lattice constant is nearly equal to that of CrN, a = 414.99 pm, differing only by Δ1.5%. In fact, CrN has been shown to grow on the (111) plane of MgO(111)[10,21] or Al_2O_3(0001)[13−19] substrates.

For fabricated CrN films exhibiting intrinsic n-type Seebeck coefficients, earlier theoretical studies have indicated that the intrinsic n-type behavior can be attributed to nitrogen vacancies.[15] Several ideas to improve the n-type TE property of CrN films have been proposed: a heterostructural composite with Cr_2N[13,22] and doping of another metal.[15,18,23] Because

Received: June 2, 2025
Revised: August 25, 2025
Accepted: August 28, 2025
Published: September 5, 2025

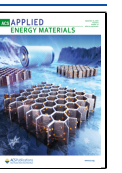

both n- and p-type legs are necessary to fabricate an efficient thermoelectric generator, fabrication of the p-type material is equally important. Therefore, an appropriate dopant or fabrication method that changes the polarity to the p-type must be found. A doping hole created by introducing V, the one-less-electron neighbor of Cr, led to n-type thermoelectricity.[15,23] Reportedly, overstoichiometry of nitrogen, i.e., Cr vacancies, can lead to holes in the valence band,[16] thereby allowing the material to gain p-type polarity, as reported for Al-doped nitrogen-overstoichiometric p-type CrN films.[14]

This work describes a newly developed effective dopant that changes the polarity of CrN thin films to p-type charge carriers. Using chemical valence bond theory, the valence of the Cr atom in CrN is +3. Therefore, we can screen simply for divalent metals as dopants. Then these dopants are screened further for appropriate bond lengths comparable to that of the Cr−N. This screening suggests Mg as an ideal dopant because of its +2 valence and bond length of 208−219 pm in Mg_3N_2, which closely matches the Cr−N bond length of 207.5 pm in CrN. Although Mg is a common dopant for the p-type group-13 nitride (GaN)[24] or group-3 nitride (ScN),[25,26] it should be confirmed by experimentation whether Mg is truly incorporated in a film at a high (1000 K) growth temperature of CrN. Our electronic structure calculations using density-functional theory (DFT) demonstrated that, in the CrN band structure, after alloying with 3.1% Mg, the Fermi energy is suppressed into the valence band, thereby changing the main charge carrier into holes. Our Mg-incorporated CrN films were grown using reactive sputtering. They showed p-type behavior, consistent with screening and calculations.

2. METHOD

CrN thin films were deposited using an ultrahigh-vacuum (UHV, base pressure approximately 2×10^{-7} Pa) magnetron sputtering system (PGS-240LS; Kenix Co. Ltd.) that can achieve simultaneous deposition (cosputtering) of up to four elements or compounds. Pure nitrogen gas (N_2) was introduced as a working and reactive gas through a mass-flow controller. As deposition sources, ϕ2-in. pure-metal targets of Cr (4N) and Mg (4N) were used. The Cr was sputtered with direct current (DC), but radiofrequency (RF, 13.56 MHz) sputtering was applied for Mg because Mg_3N_2 has a large band gap. Substrates were clamped to a sample holder plate that can be heated to 1030 K by an annular halogen lamp behind it. It is noteworthy that the substrate temperatures described hereinafter are the holder temperatures, which are higher than the true substrate temperatures. The sample holder was rotated at approximately 10 rpm during film deposition to maintain film homogeneity (thickness and composition). We used $Al_2O_3(0001)$ (epi-polished sapphire *c*-face, approximately 0.43 mm thickness; Cryscore Optoelectric Ltd.) substrates that had been ultrasonically degreased in acetone, and which were finally cleaned by heating at 1030 K in vacuum for 1 h immediately before film deposition.

Film deposition was performed under the following conditions: 1000 K substrate temperature, 100 W Cr-target DC-power, 70 mm Cr target−substrate (T−S) distance, 3 sccm N_2-gas flow rate, approximately 0.35 Pa pressure, and 1 h deposition time. The Mg was cosputtered at a 100 mm T−S distance using various amounts of RF power. The amounts are used as sample identifiers, as shown in Table 1. The supply rate of Mg_3N_2 and CrN was checked using a retractable quartz crystal microbalance (QCM) thickness monitor. The measured CrN supply rate was approximately 31 $ng \cdot cm^{-2} \cdot s^{-1}$. The calculated magnesium supply ratios in the total metal (Mg + Cr) are presented in Table 1. Under these conditions, highly optically reflective films of 200−400 nm thickness were obtained.

Table 1. Applied RF Power on a Mg Target, QCM-Measured Supply Rate for Mg_3N_2, Mg Ratio in the Total (Cr + Mg) Supply, and Real Mg Concentration in Films Measured Using HAXPES

RF power (W) (sample ID)	Mg_3N_2 rate ($ng \cdot cm^{-2} \cdot s^{-1}$)	Mg ratio (%)	Mg content (%)
#0	0	0	
#10			0.8 ± 0.1
#15			
#20			1.3 ± 0.2
#25			
#30	2.5	14	4.0 ± 0.6
#35			
#40	3.8	19	3.3 ± 0.5
#45			8.0 ± 1.2
#50	5.7	27	4.8 ± 0.7
#60	7.9	33	18.2 ± 2.7

The crystal phase and quality were checked by using X-ray diffraction (XRD) with a diffractometer (SmartLab 3; Rigaku Corp.). The film thicknesses were estimated by using a surface profilometer (Dektak 6; Bruker Analytik GmbH). The TE properties were measured using an apparatus (ZEM-3; Advance Riko Inc.). Film compositions were assessed using a hard X-ray photoelectron spectroscopy (HAXPES, PHI Quantes; Ulvac PHI Inc.) apparatus in which a monochromated Cr K_α X-ray source ($h\nu$ = 5.411 keV) was used to reduce surface contamination effects. The electron escape depth was approximately 6 nm in Cr.[27] The Mg concentrations in the total metal (Mg + Cr) amounts were calculated from the peak intensities using software (MultiPak; Ulvac PHI Inc.).

For this system, a DFT calculation was performed using VASP,[28−30] following the computational setup reported by Singh et al.[18] The same spin configuration as in Figure 1a in ref 18 is used, along with the generalized gradient approximation exchange−correlation function with Hubbard U parameter (GGA + *U*), where we introduce a *U* of 3 eV in accord with Alling et al.[31] A Perdew−Burke−Ernzerhof (PBE) formulation[32] with projector augmented-wave (PAW) ultrasoft pseudopotentials[33,34] is adopted. Calculations were performed for the primitive (rhombohedral) bulk structure and for a 2 × 2 × 2 conventional (rock-salt) supercell with a cutoff energy of 560 eV, where the respective 21 × 21 × 21 and 2 × 2 × 2 ***k***-point meshes were used to maintain a 0.02 $Å^{-1}$ spacing for all calculations. Because a 2 × 2 × 2 supercell contains 32 Cr atoms and 32 nitrogen atoms, one substitution of Cr with Mg represents 3.1% (1/32) Mg doping. The TE transport coefficients were obtained by solving the linearized Boltzmann transport equation under constant relaxation time approximation (CRTA) of $\tau = 10^{-15}$ s using the BoltzTraP2 package.[35] This τ value is roughly estimated from the measured resistivity and dopant concentration as described in the Supporting Information. A Fourier-interpolated DFT electronic band structure served as an input for the transport calculations.

https://doi.org/10.1021/acsaem.5c01663
ACS Appl. Energy Mater. 2025, 8, 13360−13366

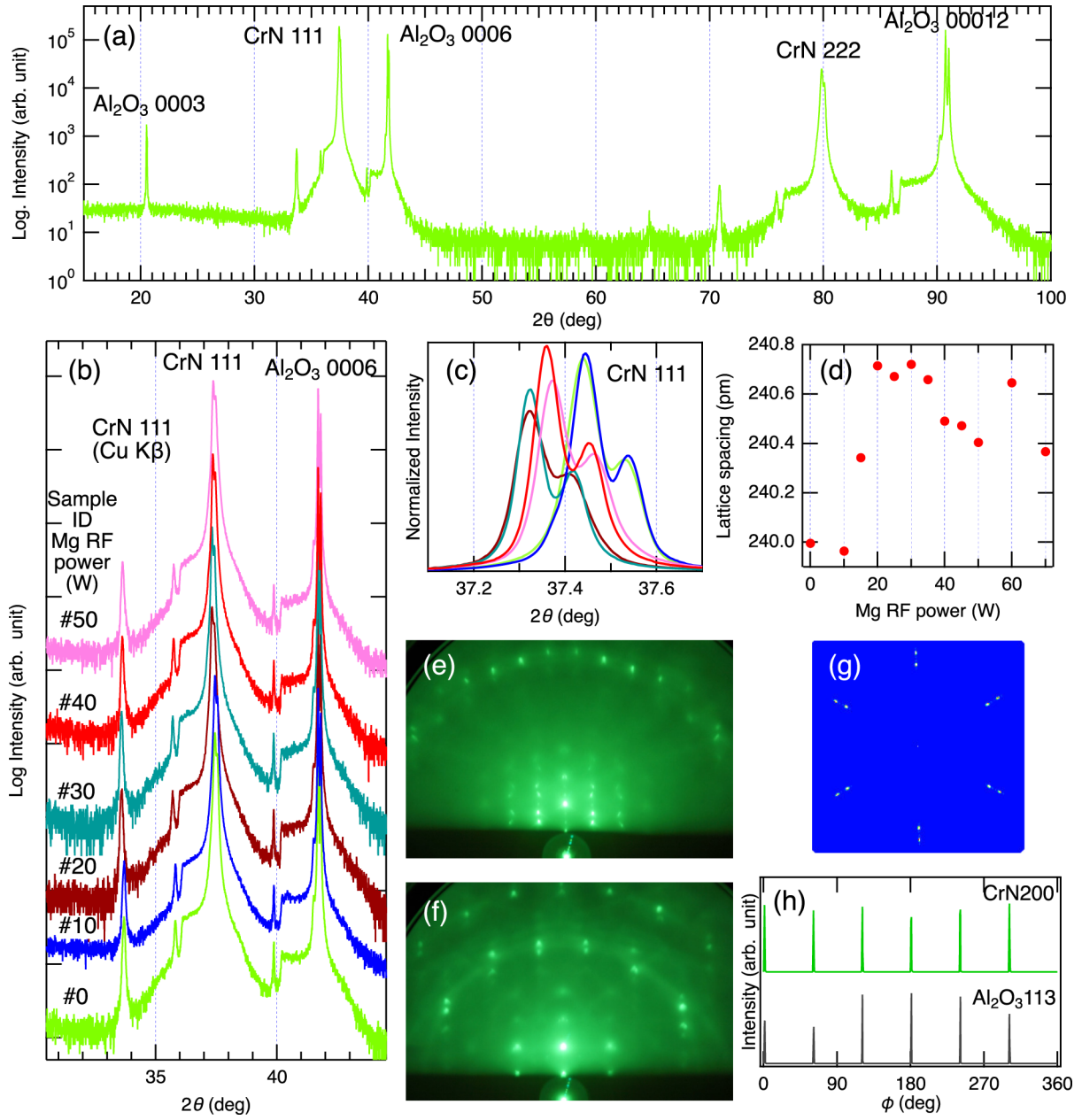

Figure 1. Panels show the following: (a) θ–2θ wide-range XRD of a pristine CrN (#0) film, (b) XRD of Mg-doped films, (c) close up of the CrN 111 peak, (d) lattice spacing calculated from the XRD peak positions, RHEED patterns for the #0 sample along (e) $\langle 1\bar{1}0 \rangle$ and (f) $\langle 11\bar{2} \rangle$ azimuths (E_0 = 15 keV), (g) XRD pole figure, where inner and outer spots respectively correspond to CrN 200 and Al_2O_3 113 diffractions, and (h) their ϕ scans.

3. RESULTS AND DISCUSSION

The XRD of the grown film showed strong CrN *nnn* (n = 1, 2) and substrate sapphire 000*m* (m = 6, 12) diffraction peaks, as exhibited in Figure 1a. No other remarkable peak was observed in either sample.

No peak was apparent around 2θ = 40.4°, which corresponds to the Cr_2N 0002 diffraction peak, indicating that the Cr_2N phase was produced only in low quantities. By contrast, when the substrate temperature was increased by 15 K, the Cr_2N phase began to appear as shown in Figure S2 in the Supporting Information. As Figure 1b,c illustrates, the CrN 111 diffraction peak shifts slightly when Mg is doped. The lattice spacings (d) are calculated from the diffraction-peak position, which increased slightly (approximately 0.3%) when Mg was incorporated. However, the values tended to saturate or decrease nonlinearly at higher Mg contents. This behavior resembles that observed for the dependence of the CrN lattice constant on the nitrogen content,[16] where the lattice constant changes steeply around the stoichiometric region during the p–n transition. The sharp diffraction peak widths indicate the high crystal quality of the films.

The reflection high-energy electron diffraction (RHEED) patterns were obtained *ex situ* for several samples that had been brought into air and transferred to another UHV chamber for RHEED observation. The RHEED pattern appeared on the as-grown samples with no additional surface-cleaning process. The RHEED patterns for sample #0 presented in Figure 1e,f are transmission patterns showing short streaky diffraction

https://doi.org/10.1021/acsaem.5c01663
ACS Appl. Energy Mater. 2025, 8, 13360–13366

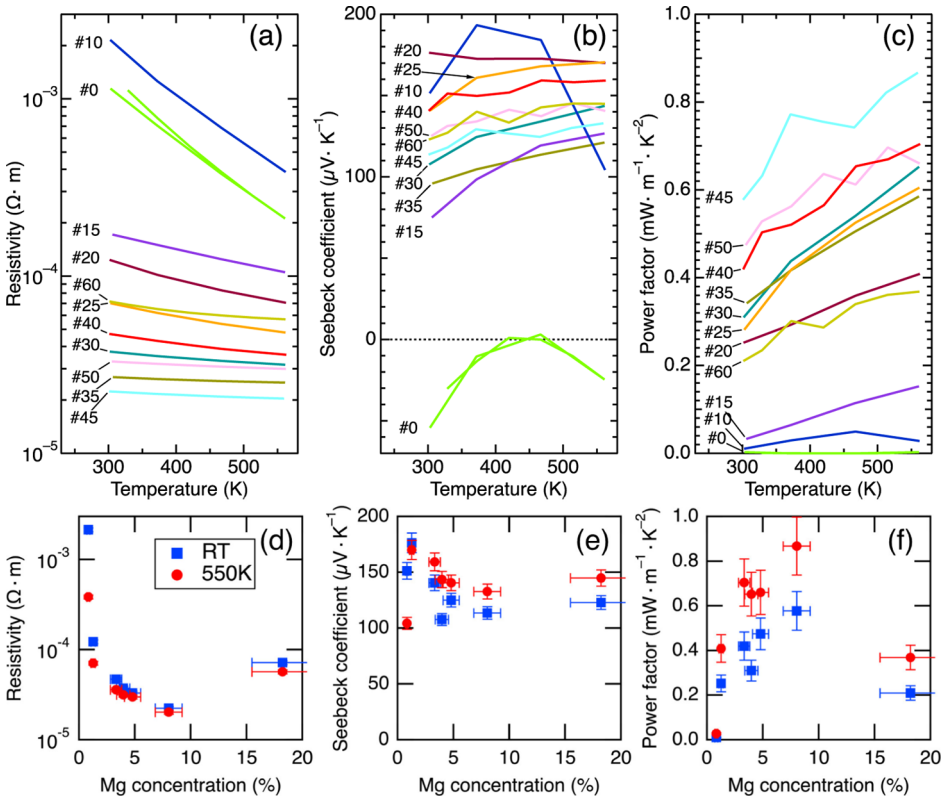

Figure 2. Measured temperature dependence of (a) resistivity, (b) the Seebeck coefficient, (c) power factor of Mg-doped CrN films, and (d–f) variations of their range with the Mg concentration in the film. Only sample #0 was measured in both ways (increasing and decreasing temperature) to check stability.

spots, indicating the rough and faceted surface. The $\langle 1\bar{1}0\rangle$ -azimuth RHEED pattern [Figure 1e] is symmetric in its diffraction pattern, but it should be asymmetric on the single-crystal rock-salt structure. The symmetric RHEED suggests a twin, two-domain structure in which 180°-rotated domains coexist, similarly to what has been reported for PLD films.[21] Similar RHEED patterns were observed for Mg-doped samples. The XRD polar scan results are shown in Figure 1g,. The two-domain epitaxial relation is confirmed: (111)CrN ∥ (0001)Al_2O_3 and [11$\bar{2}$] CrN or [$\bar{1}\,\bar{1}$2] CrN ∥ [11$\bar{2}$0]Al_2O_3. The uniform intensities of the CrN200 diffraction peaks indicate that the areas of the respective domains are almost equal.

The Mg concentrations in the metal in total (Mg + Cr) were estimated using HAXPES. The results are presented in Table 1. The substrate temperature (1000 K) was considerably high for Mg: its vapor pressure is approximately 10^3 Pa. However, once the Mg–N bond has been formed, re-evaporation is not governed by the Mg vapor pressure but instead by the Mg–N bond decomposition rate. As a result of the dynamic balance between the incoming and the re-evaporation rates, the amount of Mg found in the growing film was much less than the amount supplied. The measured Mg concentration tends to increase with the applied Mg RF power, but it is greatly scattered, probably because of several factors: First, small deviations of the substrate temperature caused by the clamping-force fluctuation might produce a strong effect because the Mg re-evaporation rate is strongly temperature-dependent. Second, precise control of the Mg deposition rate is difficult when using the reactive sputtering method because nitridation of the Mg target gradually decreases the sputtering rate. Third, background estimation in HAXPES includes a considerable degree of ambiguity, leading to non-negligible errors in the data. Successful incorporation of a few percent order of Mg was confirmed for the present experimental conditions despite the high substrate temperature during growth.

Figure 2 shows the measured TE properties. In general, the electric resistivity (a) decreases concomitantly with increasing temperature, which is a typical semiconductor feature and which is consistent with the reported resistivity for near-stoichiometric CrN films.[16,36,37] As the Mg doping level increases, the resistivity decreases rapidly, reaching a minimum at sample no. 45; it then increases gradually again. The Seebeck coefficient (b) of the pristine CrN film (no. 0) shows a bipolar feature: the polarity switches with the temperature. This behavior is similar to or slightly less pronounced than that presented in Figure 5a in ref 16 for the $CrN_{0.97}$ film on Al_2O_3(0001), suggesting that the stoichiometry of our sample should be slightly less than 0.97. At high Mg-doping concentrations, the material retains a p-type Seebeck coefficient. In most cases, the Seebeck coefficient increases with the temperature. As a result, the power factor also increases with temperature, as shown in Figure 2c. Figure 2d–f shows the dependence of each TE property at RT and 550 K against the Mg concentration measured from HAXPES. The optimum Mg concentration is approximately 5–10%, at which the resistivity becomes minimal and yields the maximum power factor around 0.6 mW·m^{-1}·K^{-2} at RT and 0.9 mW·m^{-1}·K^{-2} at approximately 550 K.

The DFT calculated electronic band is exhibited in Figure 3. The pristine CrN (a) is shown to host a direct band gap of

https://doi.org/10.1021/acsaem.5c01663
ACS Appl. Energy Mater. 2025, 8, 13360–13366

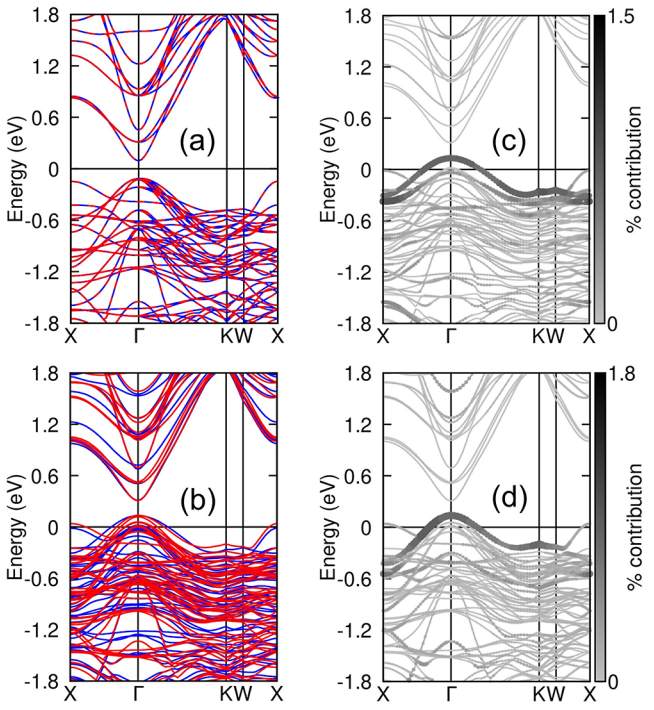

Figure 3. Calculated electronic band structure along the X−Γ−K−W−X Brillouin zone path for the 2 × 2 × 2 supercells of (a) pristine CrN and (b) CrN with 3.1% Mg-doping, and projected Mg orbitals on the (c) spin-up and (d) spin-down states. Both configurations are similar to those reported by Singh et al.,[18] with blue and red lines corresponding,, respectively to the spin-up and spin-down bands.

0.21 eV at the Γ point. This result is similar to those reported in the literature,[18] but it is not consistent with earlier optical measurements[11] or the local spin-density approximation corrected using Hubbard Coulomb term (LSDA + U) calculation,[38] in which indirect band gap has been inferred. This difference can be attributed to the antiferromagnetic spin configuration of the CrN lattice.[18] The curvature of the highest-energy valence band is broader than that of the lowest-energy conduction band, indicating that the hole effective mass is greater than that of the electron. We can calculate this analytically by fitting the dispersion, which showed an effective hole mass of 0.863 m_0 and electron effective masses of 0.233 and 0.184 m_0, respectively, along the Γ−X and Γ−K paths, for spin-up and -down channels of the pristine CrN structure. This finding related to hole mass is expected to reduce the hole mobility of the p type CrN more than the electron mobility in the n type. Using the Drude formula $\mu = e\tau/m_n^*$, where e stands for the electron charge, τ denotes the relaxation time and m^* signifies the effective mass, and assuming $\tau = 10^{-15}$ s, one can approximate mobility values of approximately 7.55 and 9.56 $cm^2/V{\cdot}s$ for electrons and 2.04 $cm^2/V{\cdot}s$ for holes. In fact, the observed p-type power factor here is smaller than the reported value in the n-type CrN,[13,15] which can be attributed mainly to the lower mobility.

The experiment elucidates the n-type behavior of the undoped CrN thin film (no. 0) in the 300−600 K range and the p-type behavior for the Mg-doped CrN. These findings actually match very well with calculated results because the difference is attributed to the temperature shift and bipolar conduction as a result of the small gap. Our doped samples with only 3.1% Mg introduced into the lattice serve to shift the band upward, thereby roughly maintaining the structure as exhibited in Figure 3b. As a result, the Fermi energy is driven deeper into the valence band, consequently enhancing the hole conductivity. The band gap in this case is reduced to 0.17 eV, as presented in Figure 3b. The hole effective mass is reduced to 1.00 m_0, whereas the electron effective mass remains approximately 0.27 m_0 along the Γ−X path and 0.21 m_0 along the Γ−K path. Using the same Drude formula, it is apparent that the mobility is reduced to 1.75 $cm^2/V{\cdot}s$ for holes and to 6.54 and 8.46 $cm^2/V{\cdot}s$ for the Γ−X and Γ−K paths. This hole carrier contribution is consistent with the calculated Seebeck result when one observes a larger temperature range (100−900 K) as in Figure 4.

With increasing temperature, it is apparent that the Seebeck coefficient shifts from p to n type in the 300−600 K range at low ($\leq 10^{19}$) hole concentrations, whereas it remains in p type at high ($\geq 10^{20}$) hole concentrations, which well matches the experimentally obtained result achieved with Mg doping. This p to n switch is attributable to the different carrier mobility in the bipolar conduction. Because electrons have a higher

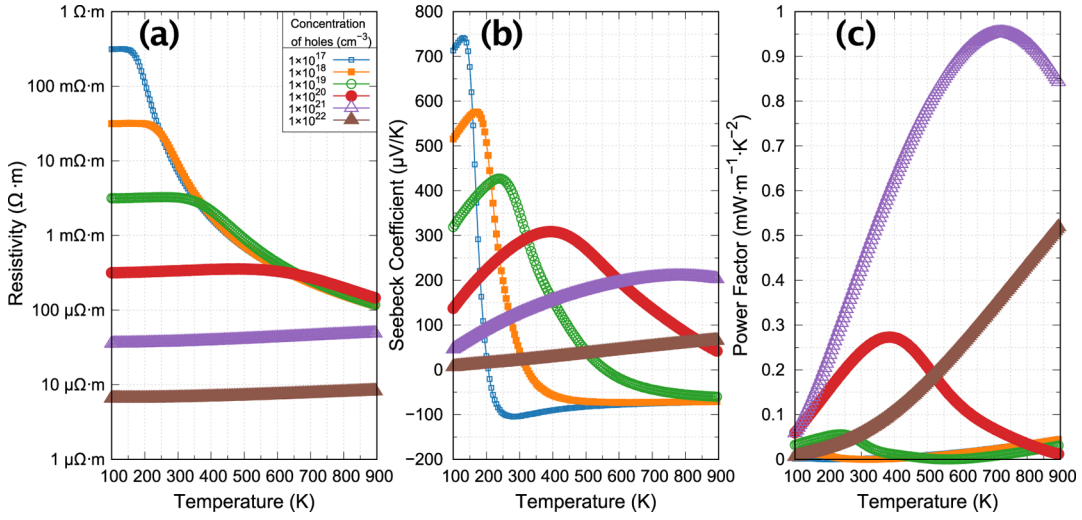

Figure 4. Calculated (a) resistivity, (b) Seebeck coefficient, and (c) power factor ($S^2\sigma$) from the interpolated electronic structure, as shown in Figure 3a for CrN at different hole doping levels. The purple triangle 10^{21} cm^{-3} curve is the most comparable with experimentally obtained results.

https://doi.org/10.1021/acsaem.5c01663
ACS Appl. Energy Mater. 2025, 8, 13360−13366

mobility than holes, their contribution becomes dominant at high temperatures, where both carriers are thermally induced. Because the CrN cell volume is $(4.15 \times 10^{-8})^3$ cm^3 for 4 Cr atoms, the doping level of 10^{21} cm^{-3} corresponds to a 1.79% substitution of a Cr atom if one dopant made one hole. The experimentally measured Mg is not completely substituted for Cr. Actually, interstitials, inclusions, and segregations at grain boundaries are possible, which are not expected to work as a dopant. Therefore, the measured 8%-Mg concentration in sample #45 presumably corresponds to the calculation for a 10^{21} cm^{-3}-hole concentration (1.79% doping): The dopant efficiency was approximately 20−25%.

4. SUMMARY

Using reactive sputtering, two-domain epitaxial CrN(111) thin films were grown on a sapphire (0001) substrate. By cosputtering, Mg can be doped from less than 1% to more than 10%, which changes the polarity at around RT from n type to p type. The maximum measured power factor was from 0.6 mW·m^{-1}·K^{-2} (RT) to 0.9 mW·m^{-1}·K^{-2} (550 K). The DFT calculations show that 3.1% Mg-substitution into Cr site shifts the electronic band upward such that the Fermi energy is in the valence band, inducing hole carriers. Calculation of the TE properties can explain the experimentally obtained results very well. This finding opens a path to providing stable p-type CrN thin films. Because the n-type CrN provides a high TE performance, it appears promising to combine both p-type and n-type CrN thin films to produce an equally high-performance TE generator.

■ ASSOCIATED CONTENT

Supporting Information

The Supporting Information is available free of charge at https://pubs.acs.org/doi/10.1021/acsaem.5c01663.

Optimizing the sputtering conditions and estimation of τ (PDF)

■ AUTHOR INFORMATION

Corresponding Authors

Takashi Aizawa − *Research Center for Materials Nanoarchitectonics, National Institute for Materials Science, Tsukuba, Ibaraki 305, Japan;* orcid.org/0000-0003-2357-5336; Email: AIZAWA.Takashi@nims.go.jp

Takao Mori − *Research Center for Materials Nanoarchitectonics, National Institute for Materials Science, Tsukuba, Ibaraki 305, Japan;* orcid.org/0000-0003-2682-1846; Email: MORI.Takao@nims.go.jp

Author

Frank F. Yun − *Research Center for Materials Nanoarchitectonics, National Institute for Materials Science, Tsukuba, Ibaraki 305, Japan*

Complete contact information is available at: https://pubs.acs.org/10.1021/acsaem.5c01663

Notes

The authors declare no competing financial interest.

■ ACKNOWLEDGMENTS

We appreciate funding provided by the JST-Mirai Program: Grant No. JPMJM19A1. Cooperation by the Surface and Bulk Analysis Unit of NIMS is acknowledged for the XRD and HAXPES measurements. A part of this work was supported by ARIM of MEXT (JPMXP1224NM5121 and JPMXP1225NM5136).

■ REFERENCES

(1) Mori, T.; Priya, S. Materials for energy harvesting: At the forefront of a new wave. *MRS Bull.* **2018**, *43*, 176−180.

(2) Chen, X.; Zhou, Z.; Lin, Y.-H.; Nan, C. Thermoelectric thin films: Promising strategies and related mechanism on boosting energy conversion performance. *J. Materiomics* **2020**, *6*, 494−512.

(3) Ohkubo, I.; Murata, M.; Lima, M. S. L.; Sakurai, T.; Sugai, Y.; Ohi, A.; Aizawa, T.; Mori, T. Miniaturized in-plane π-type thermoelectric device composed of a II−IV semiconductor thin film prepared by microfabrication. *Mater. Today Energy* **2022**, *28*, 101075.

(4) Ishii, S.; Bourgès, C.; Tanjaya, N. K.; Mori, T. Transparent thermoelectric device for simultaneously harvesting radiative cooling and solar heating. *Mater. Today* **2024**, *75*, 20−26.

(5) Yanagisawa, R.; Koike, S.; Nawae, T.; Tsujii, N.; Wang, Y.; Mori, T.; Ruther, P.; Paul, O.; Yoshida, Y.; Harashima, J.; Kinumura, T.; Inada, Y.; Nomura, M. High-power-density hybrid planar-type silicon thermoelectric generator with phononic nanostructures. *Mater. Today Phys.* **2024**, *45*, 101452.

(6) Eklund, P.; Kerdsongpanya, S.; Alling, B. Transition-metal-nitride-based thin films as novel energy harvesting materials. *J. Mater. Chem. C* **2016**, *4*, 3905−3914.

(7) Gall, D.; Shin, C. S.; Haasch, R. T.; Petrov, I.; Greene, J. E. Band gap in epitaxial NaCl-structure CrN(001) layers. *J. Appl. Phys.* **2002**, *91*, 5882.

(8) Gall, D.; Shin, C.-S. S.; Spila, T.; Odén, M.; Senna, M. J. H.; Greene, J. E.; Petrov, I. Growth of single-crystal CrN on MgO(001): Effects of low-energy ion-irradiation on surface morphological evolution and physical properties. *J. Appl. Phys.* **2002**, *91*, 3589−3597.

(9) Barshilia, H. C.; Selvakumar, N.; Deepthi, B.; Rajam, K. S. A comparative study of reactive direct current magnetron sputtered CrAlN and CrN coatings. *Surf. Coat. Technol.* **2006**, *201*, 2193−2201.

(10) Willmann, H.; Beckers, M.; Birch, J.; Mayrhofer, P. H.; Mitterer, C.; Hultman, L. Epitaxial growth of Al-Cr-N thin films on MgO(111). *Thin Solid Films* **2008**, *517*, 598−602.

(11) Zhang, X. Y.; Gall, D. CrN electronic structure and vibrational modes: An optical analysis. *Phys. Rev. B* **2010**, *82*, 045116.

(12) Harzer, T. P.; Daniel, R.; Mitterer, C.; Dehm, G.; Zhang, Z. L. Transmission electron microscopy characterization of CrN films on MgO(001). *Thin Solid Films* **2013**, *545*, 154−160.

(13) Gharavi, M. A.; Kerdsongpanya, S.; Schmidt, S.; Eriksson, F.; Nong, N. V.; Lu, J.; Balke, B.; Fournier, D.; Belliard, L.; le Febvrier, A.; Pallier, C.; Eklund, P. Microstructure and thermoelectric properties of CrN and CrN/Cr2N thin films. *J. Phys. D: Appl. Phys.* **2018**, *51*, 355302.

(14) le Febvrier, A.; Van Nong, N.; Abadias, G.; Eklund, P. P-type Al-doped Cr-deficient CrN thin films for thermoelectrics. *Appl. Phys. Express* **2018**, *11*, 051003.

(15) Gharavi, M. A.; Gambino, D.; le Febvrier, A.; Eriksson, F.; Armiento, R.; Alling, B.; Eklund, P. High thermoelectric power factor of pure and vanadium-alloyed chromium nitride thin films. *Mater. Today Commun.* **2021**, *28*, 102493.

(16) le Febvrier, A.; Gambino, D.; Giovannelli, F.; Bakhit, B.; Hurand, S.; Abadias, G.; Alling, B.; Eklund, P. p-type behavior of CrN thin films via control of point defects. *Phys. Rev. B* **2022**, *105*, 104108.

(17) Hjort, V.; Tessier, F.; Giovannelli, F.; le Febvrier, A.; Eklund, P. Influence of Ammonia Annealing on Cr−N Thin Films and Their Thermoelectric Properties. *ACS Appl. Energy Mater.* **2024**, *7*, 6785−6792.

(18) Singh, N. K.; Hjort, V.; Honnali, S. K.; Gambino, D.; le Febvrier, A.; Ramanath, G.; Alling, B.; Eklund, P. Effects of W alloying on the electronic structure, phase stability, and thermoelectric power factor in epitaxial CrN thin films. *J. Appl. Phys.* **2024**, *136*, 155301.

(19) Ney, A.; Rajaram, R.; Parkin, S. S. P.; Kammermeier, T.; Dhar, S. Magnetic properties of epitaxial CrN films. *Appl. Phys. Lett.* **2006**, *89*, 112504.
(20) Liu, Y. H.; Wang, K.; Lin, W.; Chinchore, A.; Shi, M.; Pak, J.; Smith, A. R.; Constantin, C. The effect of growth parameters on CrN thin films grown by molecular beam epitaxy. *Thin Solid Films* **2011**, *520*, 90−94.
(21) Jin, Q.; et al. Structural twinning-induced insulating phase in CrN (111) films. *Phys. Rev. Mater.* **2021**, *5*, 023604.
(22) Biswas, B.; Chakraborty, S.; Chowdhury, O.; Rao, D.; Pillai, A. I. K.; Bhatia, V.; Garbrecht, M.; Feser, J. P.; Saha, B. In-plane Cr2N-CrN metal-semiconductor heterostructure with improved thermoelectric properties. *Phys. Rev. Mater.* **2021**, *5*, 114605.
(23) Quintela, C. X.; Rivadulla, F.; Rivas, J. M. Thermoelectric properties of stoichiometric and hole-doped CrN. *Appl. Phys. Lett.* **2009**, *94*, 152103.
(24) Akasaki, I.; Amano, H.; Kito, M.; Hiramatsu, K. Photoluminescence of Mg-doped p-type GaN and electroluminescence of GaN p−n junction LED. *J. Lumin.* **1991**, *48*−*49*, 666−670.
(25) Tureson, N.; Marteau, M.; Cabioch, T.; Van Nong, N.; Jensen, J.; Lu, J.; Greczynski, G.; Fournier, D.; Singh, N.; Soni, A.; Belliard, L.; Eklund, P.; le Febvrier, A. Effect of ion-implantation-induced defects and Mg dopants on the thermoelectric properties of ScN. *Phys. Rev. B* **2018**, *98*, 205307.
(26) Saha, B.; Perez-Taborda, J. A.; Bahk, J.-H.; Koh, Y. R.; Shakouri, A.; Martin-Gonzalez, M.; Sands, T. D. Temperature-dependent thermal and thermoelectric properties of n-type and p-type Sc1-xMgxN. *Phys. Rev. B* **2018**, *97*, 085301.
(27) Tanuma, S.; Powell, C. J.; Penn, D. R. Calculations of electron inelastic mean free paths. IX. Data for 41 elemental solids over the 50 eV to 30 keV range. *Surf. Interface Anal.* **2011**, *43*, 689−713.
(28) Kresse, G.; Furthmüller, J. Efficiency of ab-initio total energy calculations for metals and semiconductors using a plane-wave basis set. *Comput. Mater. Sci.* **1996**, *6*, 15−50.
(29) Kresse, G.; Furthmüller, J. Efficient iterative schemes for ab initio total-energy calculations using a plane-wave basis set. *Phys. Rev. B* **1996**, *54*, 11169−11186.
(30) Kresse, G.; Hafner, J. Ab initio molecular dynamics for liquid metals. *Phys. Rev. B* **1993**, *47*, 558−561.
(31) Alling, B.; Marten, T.; Abrikosov, I. A. Effect of magnetic disorder and strong electron correlations on the thermodynamics of CrN. *Phys. Rev. B* **2010**, *82*, 184430.
(32) Perdew, J. P.; Burke, K.; Ernzerhof, M. Generalized Gradient Approximation Made Simple. *Phys. Rev. Lett.* **1996**, *77*, 3865−3868.
(33) Kresse, G.; Hafner, J. Norm-conserving and ultrasoft pseudopotentials for first-row and transition elements. *J. Phys.: Condens. Matter* **1994**, *6*, 8245.
(34) Kresse, G.; Joubert, D. From ultrasoft pseudopotentials to the projector augmented-wave method. *Phys. Rev. B* **1999**, *59*, 1758−1775.
(35) Madsen, G. K. H.; Carrete, J.; Verstraete, M. J. BoltzTraP2, a program for interpolating band structures and calculating semi-classical transport coefficients. *Comput. Phys. Commun.* **2018**, *231*, 140−145.
(36) Zhang, X. Y.; Chawla, J. S.; Howe, B. M.; Gall, D. Variable-range hopping conduction in epitaxial CrN(001). *Phys. Rev. B* **2011**, *83*, 165205.
(37) Batko, I.; Batkova, M.; Lofaj, F. Electrical Resistivity of CrN Thin Films. *Acta Phys. Polym., A* **2014**, *126*, 415−416.
(38) Herwadkar, A.; Lambrecht, W. R. L. Electronic structure of CrN: A borderline Mott insulator. *Phys. Rev. B* **2009**, *79*, 035125.

https://doi.org/10.1021/acsaem.5c01663
ACS Appl. Energy Mater. 2025, 8, 13360−13366